Cancer Nano (2010) 1:13–18
DOI 10.1007/s12645-010-0002-4

ORIGINAL PAPER

A core-shell nanomaterial with endogenous therapeutic and diagnostic functions

Chitta Ranjan Patra · Ying Jing · Yun-Hao Xu · Resham Bhattacharya · Debabrata Mukhopadhyay · James F. Glockner · Jian-Ping Wang · Priyabrata Mukherjee

Received: 1 February 2010 / Accepted: 13 April 2010 / Published online: 5 May 2010

Abstract In the present communication, we report the fabrication of a unique core-shell inorganic nanomaterial with potential therapeutic and diagnostic functions. It contains an iron–cobalt (FeCo) core that demonstrates magnetic resonance imaging (MRI) contrast property and a thin nanoshell of gold that inhibits the function of a pro-angiogenic growth factor, VEGF165. Au(FeCo) core-shell nanomaterials are fabricated in the gas phase and characterized using transmission electron microscopy, energy dispersive spectrum, inductively coupled plasma analysis, and MRI. Inhibition of VEGF165 function by Au(FeCo) is demonstrated against VEGF165/VPF-induced signaling cascades and proliferation of human umbilical vein endothelial cells (HUVECs). The self-contrast property of Au(FeCo) is determined in vitro by MRI after incubating HUVECs with Au(FeCo), demonstrating intrinsic contrast property of this potentially therapeutic nanomaterial. In brief, we report here the successful fabrication of an inorganic core-shell nanomaterial with potential therapeutic and diagnostic functions. It inhibits the function of VEGF165 and functions as a MRI contrast agent.

Keywords Nanoparticle · Core-shell · Angiogenesis · Gold · Diagnostics · Therapeutics

Chitta Ranjan Patra, Ying Jing, Yun-Hao Xu and Resham Bhattacharya contributed equally to this paper. Both Jian-Ping Wang and Priyabrata Mukherjee designed the experiment, led the project, and finalized the paper.

C. R. Patra · R. Bhattacharya · D. Mukhopadhyay · P. Mukherjee
Department of Biochemistry and Molecular Biology,
College of Medicine, Mayo Clinic,
Rochester, MN 55905, USA

Y. Jing · Y.-H. Xu · J.-P. Wang (✉)
The Center for Micromagnetics and Information Technologies (MINT), Department of Electrical Engineering,
University of Minnesota,
EE 4-174, 200 Union St. S.E.,
Minneapolis, MN 55455, USA
e-mail: jpwang@umn.edu

D. Mukhopadhyay · P. Mukherjee (✉)
Department of Biomedical Engineering, College of Medicine, Mayo Clinic,
Rochester, MN 55905, USA
e-mail: Mukherjee.priyabrata@mayo.edu

J. F. Glockner
Department of Radiology, College of Medicine, Mayo Clinic,
Rochester, MN, USA

1 Introduction

It is recognized that nanotechnology has the potential to play an important role in human health care including angiogenesis (Gannon et al. 2008; Goldstein et al. 1995; Goodman et al. 2004; Han et al. 2007; Hong et al. 2006; Liu et al. 2007; Paciotti et al. 2004; Patra et al. 2008a; Patra et al. 2008b; Shaw et al. 2008; Sokolov et al. 2003; Sullivan and Ferrari 2004). Vascular endothelial growth factor 165 (VEGF165) plays a major role in angiogenesis by engaging VEGFR2 on endothelial cells, turning on a number of signaling cascades leading to endothelial cell proliferation, migration, survival, etc. (Ferrara and Kerbel 2005; Folkman 2007; Folkman and Hanahan 1991; Dvorak et al. 1999). Anti-angiogenic agents presently used in the clinics exhibit serious toxicities (Bhattacharya et al. 2004; Bhattacharya et al. 2007; Mukherjee et al. 2007; Mukherjee

et al. 2005). Furthermore, monitoring the effect of anti-angiogenic therapy is also a challenge. Thus, there is a clear need to discover new anti-angiogenic molecules that will exhibit low toxicity and monitor the effect of the anti-angiogenic therapy by self-contrast. Here, we report the fabrication of a unique core-shell inorganic nanomaterial with such an endogenous therapeutic and diagnostic function. It contains an iron–cobalt (FeCo) core that demonstrates magnetic resonance imaging (MRI) contrast property and a thin nanoshell of gold that inhibits the function of a pro-angiogenic growth factor, VEGF165. It is also important to consider the possible toxic effects of this nanomaterial. Since the nanoparticles are in a core-shell structure, only gold is exposed to the cells or any outside environment, and FeCo alloy is prevented from contacting anything else but gold. It is general agreement that gold is noncytotoxic based on a range of studies about modified gold nanoparticles.

Au(FeCo) core-shell nanomaterials are fabricated in the gas phase and characterized using transmission electron microscopy (TEM), energy dispersive spectrum (EDS), inductively coupled plasma-mass spectrometry (ICP-MS) analysis. Inhibition of VEGF165 function by Au(FeCo) was demonstrated against VEGF165/VPF-induced signaling cascades and proliferation of human umbilical vein endothelial cells (HUVECs). Challenging the VEGF165 function in the presence of Au(FeCo) demonstrates the inhibition of VEGF165/VPF-induced proliferation of HUVECs and inhibition of phosphorylation of VEGF receptor 2 (VEGFR2) by this nanomaterial in a dose-dependent manner. However, FeCo alone, without a gold nanoshell, does not inhibit the VEGF165/VPF-induced proliferation of HUVECs nor does it inhibit the VEGF165/VPF-induced VEGFR2 phosphorylation. In the absence of VEGF165/VPF, either Au(FeCo) or FeCo did not affect the HUVEC proliferation, suggesting the non-toxic behavior of this nanocomposite material. In addition, the self-contrast property of Au(FeCo) was determined in vitro by MRI after incubating HUVECs with Au(FeCo), demonstrating the significant contrast behavior of the cells upon nanomaterial treatment compared to non-treated control cells or phospate-buffered saline (PBS). Furthermore, intracellular uptake studies determined by ICP demonstrate a dose-dependent uptake and contrast behavior of Au(FeCo). In brief, we report here the successful fabrication of an inorganic core-shell nanomaterial with potential therapeutic and diagnostic functions. It inhibits the function of VEGF165 and functions as a MRI contrast agent. The potential biomedical applications of this nanomaterial are enormous. In addition, the presence of a gold nanoshell endows flexibility to this material to surface modification for a wide variety of biological applications including targeting.

2 Experimental

2.1 Synthesis and characterization of Au(FeCo) and FeCo nanoparticles

The FeCo–Au core-shell nanoparticles were synthesized directly in gas phase by a novel "snapshot synthesis" method (Xu and Wang 2007, 2008). The experimental apparatus consisted of a sputtering–gas–condensation source and a deposition chamber. A Fe:Co:Au (35:15:50) composite target was used to synthesize the FeCo–Au core-shell nanoparticles. The vapor of a mixture of Fe, Co, and Au atoms was generated by sputtering process. The atoms were cooled down by the collisions between the atoms and inert gas molecules, which then nucleate and grow into nanoparticles. The core-shell structure was formed by segregating the Au to the surface of the nanoparticles through heat-assisted diffusion during synthesis. The formed nanoparticles were carried out of the source by the gas flow and collected in the deposition chamber. Polyethylene glycol (PEG)-coated glass substrates were used to collect the nanoparticles and transfer them into a solution (H_2O). Cu grids covered with amorphous carbon were used for the preparation of TEM samples.

The core-shell structure of FeCo–Au nanoparticles was confirmed by EDS line scan on a single nanoparticle. FeCo-Au nanoparticles were directly deposited on amorphous carbon covered Cu grids. Analysis was done under STEM mode on a field emission gun TEM (FEI Tecnai G2 F30) equipped with an EDS detector. Electron beam scanned across a single FeCo–Au nanoparticle by 1 nm step in the designated direction. A distribution spectrum of Fe, Co, and Au in a nanoparticle was obtained.

2.2 [^{3}H]thymidine incorporation experiments

Proliferation experiments using [^{3}H]thymidine incorporation were performed as described previously (Mukherjee et al. 2005). In brief, serum-starved HUVECs were treated with VEGF165 (10 ng/mL) either free or conjugated to different doses of Au(FeCo) or FeCo. After 24 h, cells were treated with 1 μCi of thymidine for 4 h, followed by washing in PBS, fixing the cells in cold methanol, and lysing the cells with 0.1 N NaOH. The cell lysates were read in a scintillation counter for thymidine incorporation.

2.3 Western blot analysis of VEGFR2 phosphorylation

Effect of Au(FeCo) and (FeCo) on VEGFR2 phosphorylation. Western blot analysis of phospho-VEGFR2 (p-VEGFR2) and total VEGFR2 from (1) control untreated HUVECs ,(2) A, serum-starved HUVECs were stimulated for 5 min withVEGF (10 ng/mL) as a positive control, (3–5) HUVECs treated with VEGF165 while conjugated to Au(FeCo) or (FeCo) at various

concentrations [3=100 ng, 4=1 μg, and 5=10 μg of Fe–Co–Au], and (6–8) HUVECs treated with Fe–Co at various concentrations [6=100 ng, 7=1 μg, and 8=10 μg of Fe–Co]. Afterwards, the incubation cells were lysed with RIPA buffer containing PIC and halt. Cell lysates were isolated and Western blot analysis run according to literature procedure (Mukherjee et al. 2005).

2.4 Intracellular uptake of Au(FeCo)

HUVECs were grown in 100-mm collagen-coated tissue culture plates in triplicates in EGM medium and treated with different doses of (FeCo)Au for 2 h. Afterwards, the incubation cells were washed extensively in PBS thrice. Finally, the cells were trypsinized, pooled together, thoroughly washed in PBS again, and finally resuspended in PBS for ICP analysis for gold.

2.5 Magnetic resonance imaging

Samples were evaluated on 1.5 and 3 T clinical systems (GE Twin Speed EXCITE, GE Healthcare, Waukeshau, WI). Samples contained in 1-ml microcentrifuge tubes were placed in a styrofoam tube holder which was then positioned in the center of a birdcage head coil. Following three-plane single-shot fast spin echo localizing sequences, T2* and R2* measurements were performed using a multi-echo gradient echo sequence. Eight echo times (TEs) were acquired, with the following sequence parameters: TR (repetition time) 150 ms, TE 2.6–33.8 ms, flip angle 20, bandwidth 50 kHz, slice thickness of 5 mm, field of view 14 cm, imaging matrix× 256×160, two signals averaged. An axial slice was acquired through the bottom of the sample tubes.

Calculation of T2* and R2* was performed using Cine Tool software installed on a GE Advantage Windows 4.3 workstation (GE Healthcare, Waukeshau, WI). A region of interest (ROI) encompassing the bottom of the sample tube was placed on the image with the shortest TE and then copied to the remaining seven images with progressively longer TEs. The average signal intensity of each ROI was then measured and plotted versus TE, and the resulting data were fit to the expected single exponential decay curve describing the loss of transverse magnetization in the sample to solve for T2* and R2* ($S=S_0$e -TE/T2*+S_1, where S=signal intensity in arbitrary units, S_0 and S_1 are constants, and TE is the echo time. R2*, the relaxivity, is the inverse of T2*).

3 Results and discussion

The Au(FeCo) core-shell nanoparticles were synthesized directly in the gas phase by a novel "snapshot synthesis" method (described in the "Section 2" section) (Xu and Wang 2008). A Fe:Co:Au (35:15:50) composite target was used to synthesize the FeCo-Au core-shell nanoparticles and collected in the deposition chamber of PEG-coated glass. The nanoparticles thus obtained were transferred to water and characterized by TEM. Figure 1 represents the TEM micrographs of Au(FeCo) and FeCo nanoparticles. The average size of the Au(FeCo) core-shell nanoparticles is 25.36 nm, with a standard deviation of 1.92 nm (Fig. 1a, b). The composition is $(Fe_{70}Co_{30})_{50}Au_{50}$ atomic percent. For comparison, $Fe_{70}Co_{30}$ nanoparticles with natural oxide shell were also used (Fig. 1c, d). Core-shell structure is further confirmed by composition mapping of a single core-shell nanomaterial. Figure 2 shows the composition mapping of a single Au(FeCo) nanoparticle. Uniformly distributed Au shell is confirmed. EDS scan was conducted along the direction indicated by the red line (Fig. 2a). It could be seen from Fig. 2b that FeCo forms the core while Au is dominantly in the shell for the investigated nanoparticle. The highly uniform morphology of these Au (FeCo) nanoparticles (Fig. 1a, b) suggests that composition variation should be small and the diffusion of Au element to a similar extent in each particle. Therefore, the universal FeCo-Au core-shell structure is obtained.

To determine the effect of these nanoparticles to inhibit VEGF165 function, VEGF165-induced proliferation of HUVECs was performed in the presence and the absence of Au(FeCo) and FeCo (details are in the "Section 2"). Figure 3 represents the VEGF165-induced proliferation of HUVECs in the presence or absence of Au (FeCo) and FeCo. The figure clearly demonstrates a significant induction of proliferation (~threefold) when HUVECs were stimulated with 10 ng/ml VEGF165. VEGF165-induced proliferation of HUVECs was significantly inhibited (nearly 50%) in the presence of Au (FeCo), confirming the inhibition of VEGF165 function by Au(FeCo). In the absence of VEGF165, either Au (FeCo) or (FeCo) did not affect the basal HUVEC proliferation, suggesting the non-toxic behavior of these nanomaterials. Moreover, FeCo core alone did not inhibit the VEGF165-induced proliferation of HUVECs (Fig. 3b). These results confirm that the inhibition of VEGF165 function is due to the gold nanoshell present in Au(FeCo) and not due to the (FeCo) core.

To further confirm whether the inhibition of HUVEC proliferation was due to inhibition of VEGF165 function by Au(FeCo), we investigated the downstream signaling events induced by VEGF165. It is established that VEGF165 engages VEGFRs on endothelial cells leading to receptor dimerization and subsequently receptor phosphorylation at different tyrosine residues (Mukherjee et al. 2005) Therefore, we wanted to test whether treatment of HUVECs with Au (FeCo) and FeCo had any effect on VEGFR2 phosphorylation (details are in the "Section 2"). VEGF165-induced

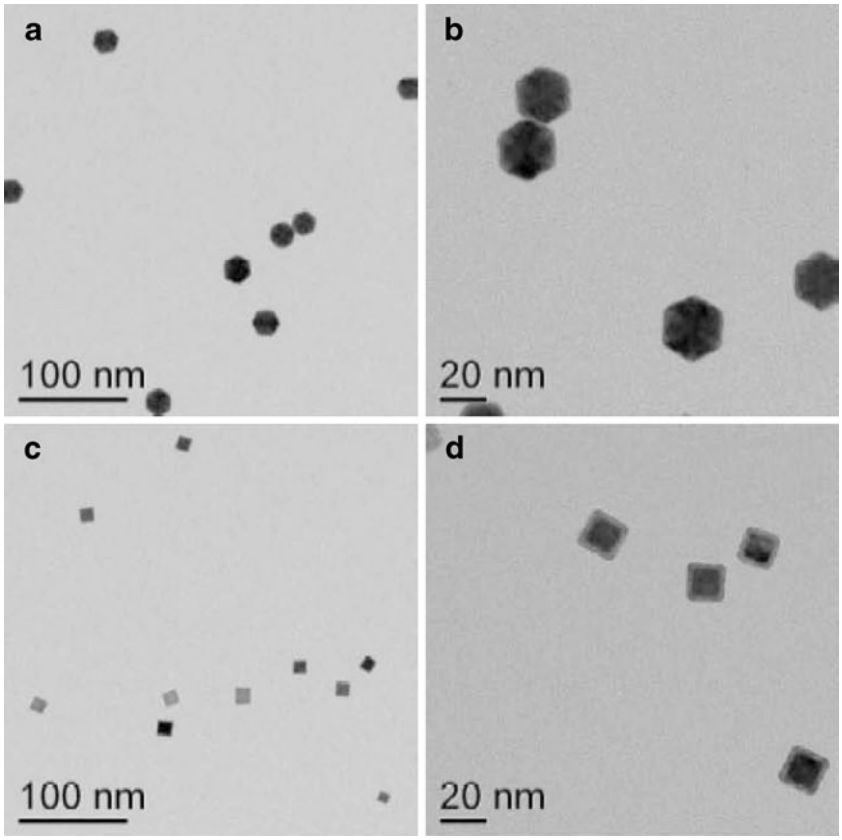

Fig. 1 TEM micrographs of Au (FeCo) and FeCo nanoparticles. **a**, **b** Low- and high-magnification images of Au (FeCo) nanoparticles, respectively. **c**, **d** Low- and high-magnification images of FeCo with natural oxide cell

phosphorylation of VEGFR2 was significantly inhibited when HUVECs were treated with 100 ng–10 μg of Au (FeCo) (Fig. 3c). However, under similar conditions, same doses of FeCo had no significant effect on VEGFR2 phosphorylation, further confirming our observation obtained from HUVEC proliferation experiments. The inhibition of VEGFR2 phosphorylation suggests that Au(FeCo) directly binds to VEGF165 and inhibits its function, leading to abrogation of receptor phosphorylation. These results are in agreement with our previous reports on the anti-angiogenic property of gold nanoparticles (Bhattacharya et al. 2004; Mukherjee et al. 2005; Bhattacharya and Mukherjee 2008). However, we do not rule out the possibility of the involvement of other mechanisms as well that will be investigated in the future.

After confirming the inhibition of VEGF165 function by Au(FeCo), we wanted next to determine the imaging

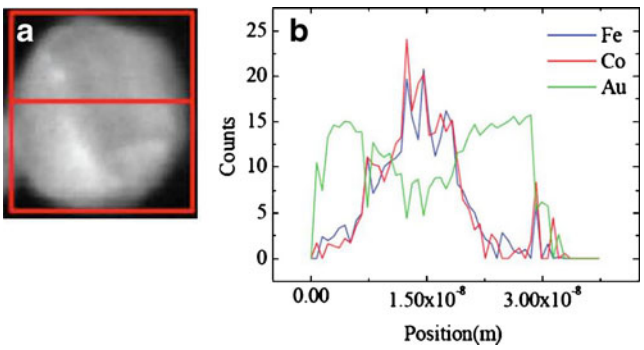

Fig. 2 Elemental mapping of a core-shell nanomaterial. **a** The HADDF image of a Au(FeCo) nanoparticle that was analyzed by EDS line scan. **b** Distribution of Fe, Co, and Au element in the nanoparticle

Fig. 3 Effect of Au(FeCo) and (FeCo) nanoparticles on VEGF165-induced proliferation of HUVECs at various concentrations (0.1–10 μg/mL), observed by [^{3}H]thymidine incorporation (cell proliferation) assay, presented as fold of stimulation. **a** VEGF165-induced proliferation of HUVECs in the presence of Au(FeCo). Au(FeCo) nanoparticles were pre-incubated with and without VEGF (10 ng/mL) for 30 min at 4°C, added to HUVEC starved with (0.1% serum) for 24 h in 24-well plates, and incubated for 24 h. After 24 h of incubation with nanoparticles, 1 μCi [^{3}H]thymidine was added into each well. Four hours later, cells were washed with cold PBS, fixed with 100% cold methanol, and the lysate collected with 0.1(N) NaOH for measurement of radioactivity. Experiments were repeated in triplicate. **b** VEGF165-induced proliferation of HUVECs in the presence of (FeCo). Experiments were performed similarly as described above. **c** Western blot analysis of VEGFR2 upon nanoshell treatment. Effect of Au(FeCo) and (FeCo) on receptor phosphorylation. Western blot analysis of phopho-KDR (p-VEGFR2) and total KDR (VEGFR2) from (*1*) control untreated HUVECs, (*2*) A, serum-starved HUVECs were stimulated for 5 min withVEGF (10 ng/mL) as a positive control, (*3–5*) HUVECs treated with Fe–Co–Au at various concentrations [3=100 ng, 4=1 μg, and 5=10 μg of Fe–Co–Au], and (*6–8*) HUVECs treated with Fe–Co at various concentrations [6=100 ng, 7=1 μg, and 8=10 μg of Fe–Co]

property of this nanomaterial. We resorted to MRI technique as FeCo has the highest saturation magnetization. Cells are treated with different doses of Au(FeCo) and fixed in formalin before imaging.

The results are shown in Fig. 4a where R2* (relaxivity) is plotted against different doses of sample at 3 T. When cells were treated with Au(FeCo), a dose-dependent increase in R2* and a progressive decrease in T2* (the

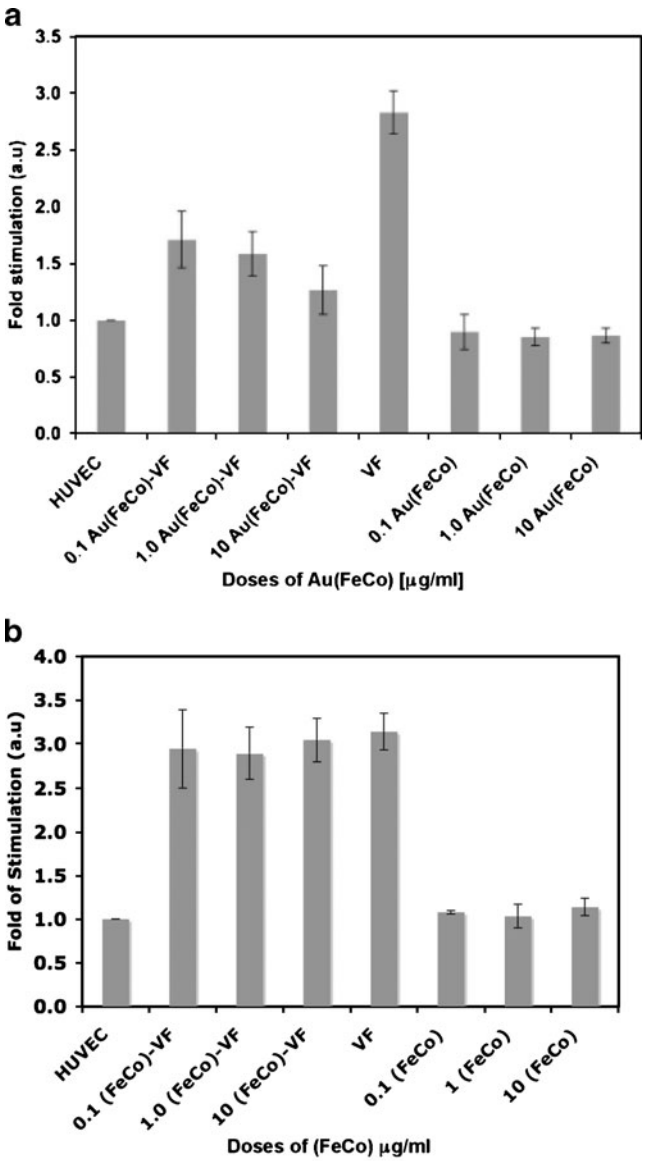

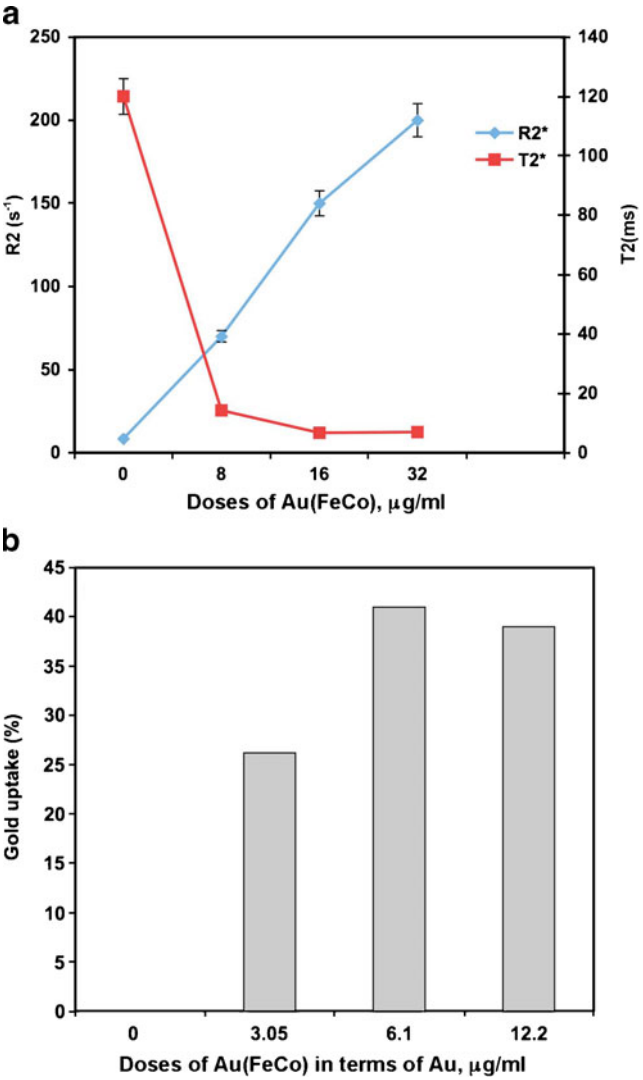

Fig. 4 Intracellular uptake and MRI experiments with HUVECs treated with Au(FeCo). Figure 4a showing the plot of R2* and T2* against sample doses exhibiting significant relaxivity of Au(FeCo) and cells treated with the same (**a**). Cells were treated with different doses of (FeCo)Au for 2 h followed by extensive washing in PBS, finally fixed in 4 % formalin before MRI. **b** Intracellular uptake of (FeCo)Au in terms of Au content. HUVECs were grown in 100 mm collagen-coated tissue culture plates in triplicates and treated with different doses of (FeCo)Au for 2 h, washed extensively in PBS thrice. Finally, the cells were trypsinized, pooled together, thoroughly washed in PBS again, and finally resuspended in PBS for ICP analysis for gold

time constant describing the rate at which the phase coherence of spins in the transverse plane decays following an initial radiofrequency pulse) values were obtained before reaching a plateau at ~32 µg/ml, clearly confirming that Au (FeCo) retains its MRI contrast properties after treatment with cells (Rad et al. 2007) Furthermore, R2* values were significantly higher in the cells incubated with nano-particles compared with the control cell samples, indicating the potential of these nanoparticles to serve as MR contrast agents.

FeCo cores of Au(FeCo) nanoparticles induce local magnetic field inhomogeneities which in turn cause a significant reduction in T2* (Rad et al. 2007; Bai and Wang 2005). This, in turn, means that samples with smaller values of T2* (or longer values of R2*) reflecting higher concentrations of iron will show more rapid signal decay on images with successively longer TEs. While many factors affect the intrinsic tissue relaxation times, the presence of iron typically represents the dominant contribution, and therefore measurements of T2* or R2* (relaxivity, or the inverse of T2*) can be related to the tissue concentration of iron (Alustiza et al. 2004). It may be noted that T2* does not decrease as much and its nearly reaching a plateau around 32 μg/ml may be due to the saturation uptake of the nanomaterial by the HUVECs. This is further confirmed by quantifying intracellular uptake of the core-shell materials in HUVECs by ICP analysis in terms of gold content. Figure 4b describes the dose-dependent uptake of the core-shell nanomaterials in terms of gold. The figure clearly demonstrates that the intracellular uptake reaches a plateau between 16 and 32 μg/ml of the core-shell nanomaterial (~6–12 μg/ml in terms of Au). Thus, there is no further significant decrease in T2* beyond these points.

4 Conclusions

Taken together, the results confirm that the core-shell nanoparticles presented in this report are intrinsically multifunctional. Our results demonstrate the fabrication of Au (FeCo), a core-shell inorganic nanoparticle, containing potential therapeutic as well as diagnostic functions. Au (FeCo) inhibits the function of pro-angiogenic VEGF165 and hence inhibits VEGF165-induced proliferation of HUVECs and inhibits VEGFR2 phosphorylation. In vitro imaging by MRI confirms the self-contrast behavior of this nanomaterial and demonstrates the significant relaxation of the cells when treated with Au(FeCo) compared to control cells and PBS. To the best of our knowledge, this nanoparticle represents the first example of an inorganic nanoparticle with endogenous dual functionality. Thus, this nanomaterial can be used as a diagnostic as well as a therapeutic agent. In the future, this theranostic material may be utilized not only for the therapeutic and diagnostic application of angiogenesis-dependent disorders but may also help to monitor the effect of the treatment on the disease outcome.

Acknowledgment This work is supported by STATE-1 (MEDICA), CA135011, CA136494 grant to PM. This work is also supported by National Science Foundation BME 0730825, NSF NNIN program, the Medical Device Center of Institute of Engineering in Medicine and Center for Nanostructures Application at University of Minnesota and Minnesota Mayo Nanotechnology Partnership for JPW.

References

Alustiza JM, Artetxe J, Castiella A, Agirre C, Emparanza JI, Otazua P, Garcia-Bengoechea M, Barrio J, Mujica F, Recondo JA (2004) Radiology 230:479–484
Bai JM, Wang JP (2005) Appl Phys Lett 87:152502–152504
Bhattacharya R, Mukherjee P (2008) Adv Drug Del Rev 60:1289–1306
Bhattacharya R, Mukherjee P, Xiong Z, Atala A, Soker S, Mukhopadhyay D (2004) Nano Lett 4:2479–2481
Bhattacharya R, Patra CR, Verma R, Kumar S, Greipp PR, Mukherjee P (2007) Adv Mater 19:711–716
Dvorak HF, Nagy JA, Feng D, Brown LF, Dvorak AM (1999) Curr Top Microbiol Immunol 237:97–132
Ferrara N, Kerbel RS (2005) Nature 438:967–974
Folkman J (2007) J Pediatr Surg 42:1–11
Folkman J, Hanahan D (1991) Princess Takamatsu Symp 22:339–347
Gannon CJ, Patra CR, Bhattacharya R, Mukherjee P, Curley SA (2008) J Nanobiotechnology 6:2
Goldstein NI, Prewett M, Zuklys K, Rockwell P, Mendelsohn J (1995) Clin Cancer Res 1:1311–1318
Goodman CM, McCusker CD, Yilmaz T, Rotello VM (2004) Bioconjug Chem 15:897–900
Han G, Ghosh P, Rotello VM (2007) Nanomed 2:113–123
Hong R, Han G, Fernandez JM, Kim BJ, Forbes NS, Rotello VM (2006) J Am Chem Soc 128:1078–1079
Liu Y, Shipton MK, Ryan J, Kaufman ED, Franzen S, Feldheim DL (2007) Anal Chem 79:2221–2229
Mukherjee P, Bhattacharya R, Wang P, Wang L, Basu S, Nagy JA, Atala A, Mukhopadhyay D, Soker S (2005) Clin Cancer Res 11:3530–3534
Mukherjee P, Bhattacharya R, Bone N, Lee YK, Patra CR, Wang S, Lu L, Secreto C, Banerjee PC, Yaszemski MJ, Kay NE, Mukhopadhyay D (2007) J Nanobiotechnology 5:4
Paciotti GF, Myer L, Weinreich D, Goia D, Pavel N, McLaughlin RE, Tamarkin L (2004) Drug Deliv 11:169–183
Patra CR, Bhattacharya R, Mukhopadhyay D, Mukherjee P (2008a) J Biomed Nanotech 4:99–132
Patra CR, Bhattacharya R,Wang E, KataryaA, Lau JS, Dutta S, Muders M, Wang S, Buhrow R, Safgren S, Yaszemski MJ, Reid JM, Ames MM, Mukherjee P, Mukhopadhyay D (2008b) Cancer Res 68:1970–78
Rad AM, Arab AS, Iskander ASM, Jiang Q, Soltanian-Zadeh H (2007) J Magne Reson Imag 26:366–374
Shaw SY, Westly EC, Pittet MJ, Subramanian A, Schreiber SL, Weissleder R (2008) Proc Natl Acad Sci U S A 105:7387–7392
Sokolov K, Follen M, Aaron J, Pavlova I, Malpica A, Lotan R, Richards-Kortum R (2003) Cancer Res 63:1999–2004
Sullivan DC, Ferrari M (2004) Mol Imaging 3:364–369
Xu Y-H, Wang J-P (2007) Appl Phys Lett 91:233107
Xu Y-H, Wang J-P (2008) Adv Mater 20:994